



# **Thermal Properties of Power Terminals in High Power IGBT Modules**

Presented at the PCIM Conference 2005, June 2005, Nürnberg, Germany by An Cosaert (Rogers NV) and Martin Wölz (Eupec, Germany)

# Thermal Properties of Power Terminals in High Power IGBT Modules

A. Cosaert<sup>1</sup>, M. Beulque<sup>1</sup>, M. Wölz<sup>2</sup>, O. Schilling<sup>2</sup>,  
H. Sandmann<sup>2</sup>, R. Spanke<sup>2</sup>, K. Appelhoff<sup>2</sup>

<sup>1</sup> Rogers NV, Gent, Belgium  
<sup>2</sup> eupec GmbH, Warstein, Germany

## Abstract

Power dissipation in the leads of IGBT modules has to be taken into account for modern inverter design. This is due to the fact that the total losses of the semiconductors are continuously decreasing while current density increases. This work analyzes the heat budget of the power terminals and the inverter interconnections. Different concepts are discussed for power terminals in high power IGBT modules. The internal connections between terminals and substrates by means of solder joints and wire bonds are compared in thermal and mechanical aspects. The basic concepts are illustrated with simulation models, and the most effective design for high current modules is deduced. The thermal and mechanical characteristics of the IHM A module and the next generation of IHM B modules are compared by both experiment and theoretical modeling. We discuss the necessity to dissipate heat from the power terminal to the heat sink and to the busbar. Static and transient design criteria for busbars are shown.



Figure 1: IHM A module and busbar

## Introduction

Progress in IGBT technology has led to a significant increase in output power since the introduction of the first High Power IGBT Module ten years ago. With the IHM A module, which is shown in Figure 1 with a typical traction busbar, an industry standard has been established that

supported a doubling in nominal module current and inverter output current without changes to the external module layout. This was possible because the dynamic and static losses of the IGBT chips have decreased with respect to the inverter output current, as shown in Figure 2. Since the packaging has remained largely unchanged, the losses due to electric lead resistance have doubled their share of the total losses.

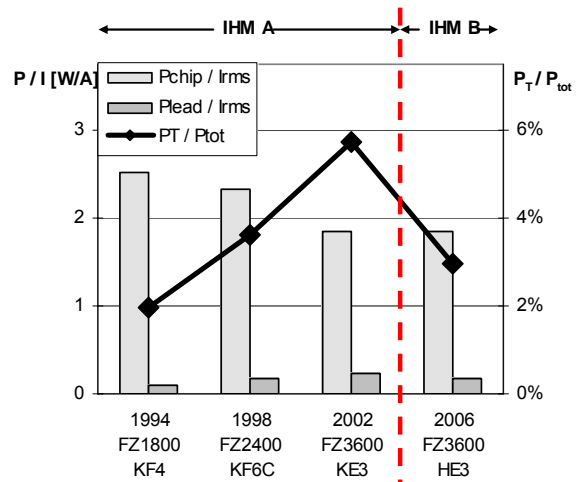


Figure 2: Total and lead losses for eupec 1700V IGBT modules. Terminal losses  $P_T$  decrease with IHM B.

In future module and inverter designs, the heat, which is dissipated by the power terminals, has to be taken into account. First, lead cross sections have to be increased in order to minimize conduction losses but without compromising mechanical flexibility and solder reliability. Second, heat flow has to be guided by reducing the thermal resistance between power terminal and heatsink and by quantifying the heat flow through the busbar. Following these principles, eupec has designed the next generation of high power modules, the IHM B type, with improved current-carrying capability.

Equally important are the advances in busbar connection technology made by Rogers NV. In the past, busbars were used as small copper bars carrying rather low current values. Typical dimensions for laminated busbars were: length = 15 x width for thicknesses of about 2mm. Due to changes in applications, current values have increased significantly, resulting in optimization of dimensions towards a trend of now length = 1.5 x width for thicknesses now up to 6mm. This increase in cross section enables control of temperature rise when carrying current.

In practice, the maximum temperature in the system is limited by the reliability of the module's internal components and the busbar. The maximum busbar temperature is 105°C for a typical insulation material such as Rogers R 8124.2. For an optimal design, both heat generation and thermal resistances have to be minimized. We start with a discussion of basic power terminal concepts, which are evaluated by FEM simulations of simplified models. Then we describe the actual behaviour of an existing IHM A module and the improvements made in the design of its successor, the IHM B. Finally, we analyze the heat budget of an inverter's entire power connection system, including both the module and the laminated busbar.

### Basic concepts and models for power terminals

In most existing IGBT modules, the power terminals are internally connected to the chips or the substrate metallization by solder joints or wire bonds. For simulation and comparison purposes, we have created a standard set of simple models, as shown in Figure 3. All models have a width of 20mm, a height of 30mm and a simplified M8 connection hole, which is typical for high power modules. The thermal simulation is carried out using ANSYS Professional(TM) 8.0

with hexahedral elements (type 69). The connection to the substrate is kept at  $T_{min}=90^{\circ}C$  and a direct current is fed through the substrate and busbar interfaces. Heat flow is allowed to dissipate by no other means but through the substrate for all these models.

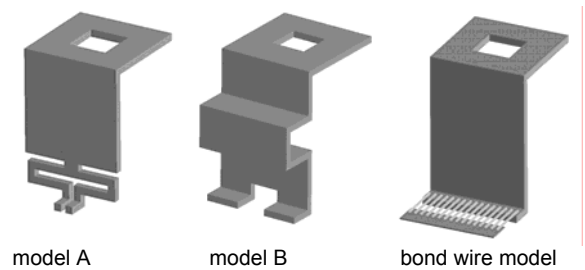


Figure 3: Basic power terminal concepts

Model A has meanders to reduce stiffness and thereby increase the reliability of the solder joint. They lie in the main plane and can be shaped in one cutting process. The copper thickness and meander width is 1.5mm. When the temperature at the busbar interface is allowed to float, assuming heat flow to the substrate only, it reaches a maximum of  $T_{max}\approx 200^{\circ}C$  at  $I=300A$ . Without dissipating heat from the power terminal to the busbar, the maximum temperature for many insulation materials would be exceeded. From the temperature distribution in Figure 4, it can be seen, that the biggest temperature gradient is observed in the meander.

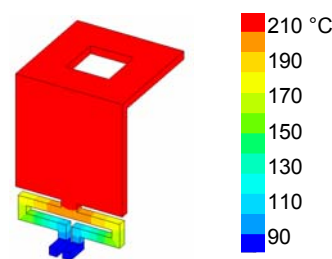
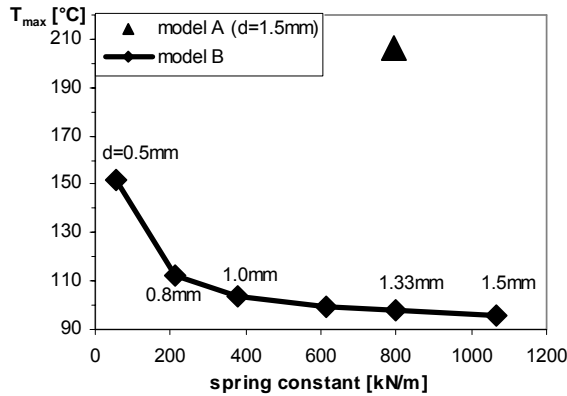


Figure 4: Model A at 300A, comparable results for model B and bond wire model shown in Figure 5 and Figure 6

Model B is aiming at a reduced temperature gradient. The thermal contact to the substrate is improved by additional solder area, and the meander is shaped by bending without reducing the width. In order to achieve the same mechanical properties as in model A, the spring constant is calculated as the elastic deformation under a vertically applied force. With a reduction in copper thickness  $d$  from 1.5mm to 1.3mm, the spring constant can be matched. With this design, the temperature gradient is reduced drastically, which is shown as a trade-off curve in Figure 5. For the same conditions as above ( $T_{min}=90^{\circ}C$ ,

$I=300A$ ), we get a maximum temperature  $T_{max}$  of only  $100^{\circ}C$ . The maximum busbar temperature of  $105^{\circ}C$  is exceeded only when the thickness is reduced below  $1.0mm$ . Model B fulfills both requirements, a low temperature rise and mechanical flexibility, better than model A.



**Figure 5: Temperature gradient and spring constant for model B at 300A**

In the bond wire model, the power terminal is connected to a metal surface by aluminum wires, taking as much room laterally as the solder connection in model B. The bond diameter is  $400\mu m$  and 16 wires are used in parallel.  $T_{min}$  is kept again at  $90^{\circ}C$  to represent bond connection to the substrate surface. If the power terminals were connected directly to the chips, the base temperature could instead be as high as  $T_{j,max}$ . The simulation results presented in Figure 6 show that the maximum temperature reached at the top of the terminal depends on the length of the bond wire.

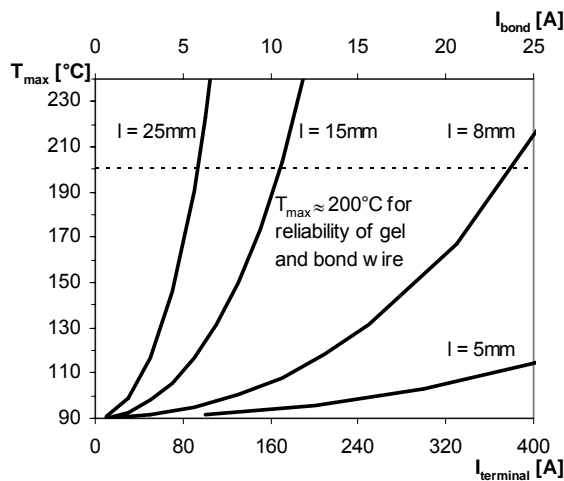


**Figure 6:  $T_{max}$  bond wire model as a function of wire length ( $l$ ) and current,  $T_{min}=90^{\circ}C$ ,  $400\mu m$  Al wire**

To deliver comparable results to model A with  $T_{max}=200^{\circ}C$  at  $I=300A$ , the bond wire length must

be reduced to  $l \approx 9mm$ . In practice, the temperature limit for wire bond reliability is around  $200^{\circ}C$ , so the maximum current per terminal and per bond wire can be read from intersections of the curves for various bond lengths.

So far, we have neglected heat transfer from the power terminal to the busbar, and  $T_{max}$  was reached on the busbar interface of the model. If we assume that the interface temperature is kept at  $T_B=105^{\circ}C$ ,  $T_{max}$  is shifted to the bond wires. The temperature distribution for  $l=25mm$  is shown in Figure 7. With  $I=180A$  the bond wires reach their maximum temperature of  $T_{max}=200^{\circ}C$ . A heat flow of  $8W$  is then dissipated through the busbar, which is determined in the simulation by integrating the heat current density across the terminal close to the interface.

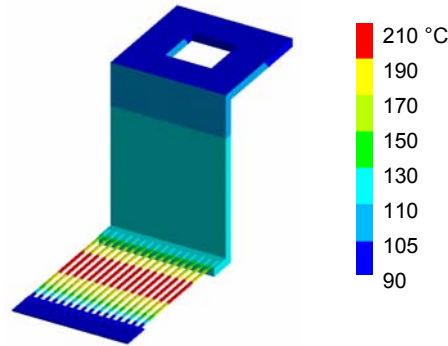


**Figure 7: Temperature distribution in bond wire model,  $d=400\mu m$ ,  $l=25mm$ ,  $h=30mm$ ,  $I=180A$ ,  $T_{min}=90^{\circ}C$ ,  $T_{bb}=105^{\circ}C$ ,  $T_{max}=200^{\circ}C$**

The discussion of these basic models leads to a systematic approach to optimize the thermal properties and reliability of power terminals. Terminal constructions with solder joints offer a good thermal behaviour and can be adapted to carry very high currents. Bond wires can be used if they are short and if their temperature is kept low at both ends. They are suitable for medium power applications.

### Power terminal concepts for next generation IHM B module compared to existing IHM A

Figure 8 shows a simplified thermal network for the power terminal assembly. Heat is generated in the busbar and in the power terminal. It flows away from the hottest point in the system with temperature  $T_{max}$  to the heatsink and the ambient air. To describe the cooling of the terminal through the heatsink, thermal resistances may be introduced:

$R_{thSC}$  is between the power terminal connection to the substrate and the module case.  $R_{thSC}$  is

determined by the terminal geometry, the connection technique and the ceramics for insulation from the baseplate.

$R_{thCH}$  between module case and heatsink is determined by the thermal grease and heat spreading.

These thermal resistances can be found by simulations and measurements in which heat transfer to the busbar is avoided. They then result from:

$$\Delta T = R_{th} \cdot P_T = R_{th} \cdot U_T \cdot I \quad (1)$$

where  $U_T$  is the voltage drop across the terminal.

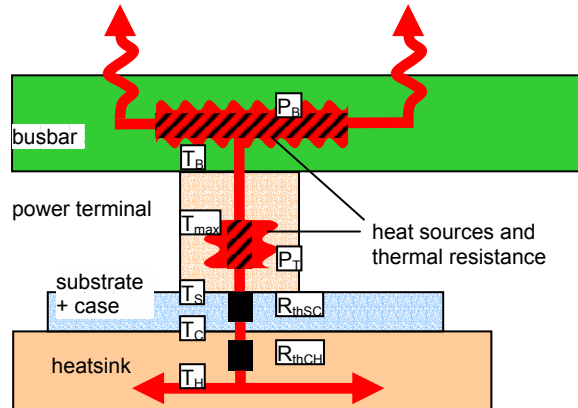


Figure 8: Thermal network of power terminal

The terminals in the current IHM A are connected to the substrate by a solder joint and have a meander in the main plane for mechanical decoupling of external forces. The assembly is shown in Figure 9. The collector and emitter terminals are identical and modeling one of them is sufficient for simulation purposes.

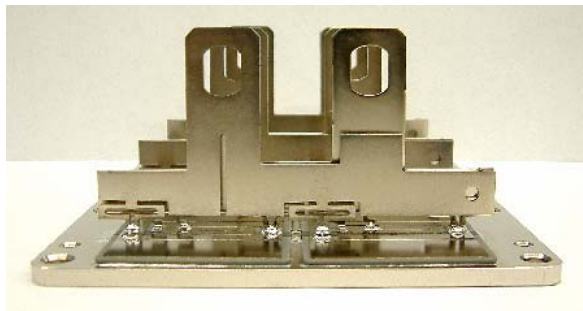


Figure 9: IHM A power terminals

In Figure 10 the calculated temperature distribution is shown for  $I=300A$  and a heatsink temperature  $T_H=80^\circ C$  with no dissipation to the busbar. As expected, the biggest thermal gradient is in the meanders above the solder joints. In the model, current is fed through a circular area of 17mm diameter around the busbar connection, which corresponds to the

contact surface. From the ANSYS calculation results, the values  $U_T$  and the temperatures  $T_S$ ,  $T_C$  and  $T_H$  were extracted.  $R_{thSC}$  and  $R_{thCH}$  can be established with (1) and are given in Table 1.  $R_{lead} = U_T / I$  is also given. Experimental results as described later could be matched by assuming convection with a film coefficient of  $\alpha = 6W/m^2K$  that takes into account that heat is also transferred to ambient air through the vertical faces of the terminal.

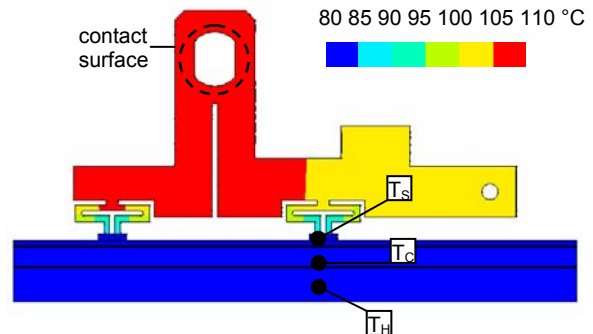


Figure 10: Temperature distribution in IHM A power terminal,  $I=300A$ ,  $T_H=80^\circ C$

For the next generation of modules, the IHM B, the meanders were eliminated and bends introduced for mechanical decoupling. This should reduce  $R_{lead}$  and thus the thermal gradient. Additionally,  $R_{thSC}$  was reduced by increasing the contact surface between terminals and substrate metallization. Another difference is the circular connection hole which provides a better contact surface to the busbar as opposed to the oblong holes in the IHM A. [3] Figure 11 shows the temperature distribution for the new design with the same conditions as above.  $T_{max}$  is reduced from  $105^\circ C$  to  $94^\circ C$ .

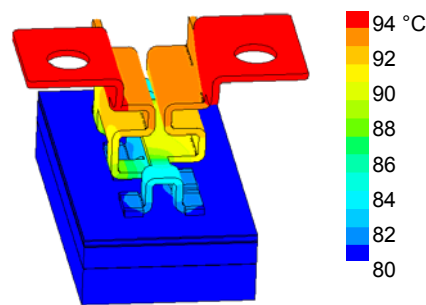


Figure 11: Temperature distribution in IHM B power terminals,  $I=300A$ ,  $T_H=80^\circ C$

The properties of the IHM B terminals as calculated with ANSYS are compared to the IHMA in Table 1. The electrical resistance is decreased by 50%, leading to less power dissipation as shown in Figure 2. The thermal resistance  $R_{thSC}$  is improved by a factor of 5.

	$R_{lead}$ [m $\Omega$ ]	$R_{thSC}$ [K/W]	$R_{thCH}$ [K/W]
IHM A	0.22	0.35	$\approx 0.05$
IHM B	0.11	0.07	$\approx 0.05$

**Table 1: Power terminal properties under load, extracted from ANSYS modeling,  $T_H=80^\circ\text{C}$ ,  $I=440\text{A}$**

Experiments were carried out to confirm the calculation results. In order to exclude heat flow from the top of the terminals to a busbar, special modules with IHM A and IHM B terminals were built in which the current is fed into the terminals only through the substrates. A short circuit bar is placed across the collector and emitter terminal. In this way, heat from the terminal can flow only through the module baseplate, just like the simulation assumes. Figure 12 shows the assembly for the IHM B terminal.

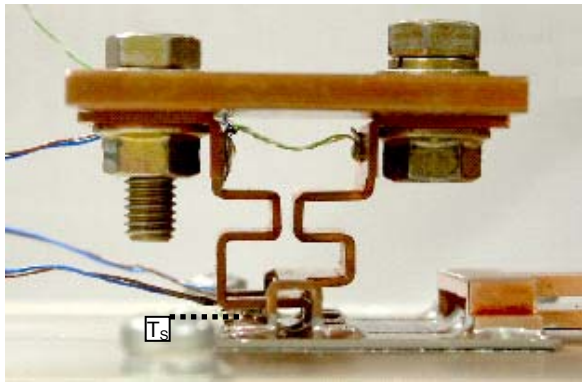


**Figure 12: Experimental setup for IHM B power terminal with short-circuit bar**

Thermocouples are placed in the same positions as the temperature reading points in the simulation. During the measurement, ventilation is blocked with insulation material. Readings are taken after the system has stabilized, and the  $R_{th}$ -values from Table 1 can be confirmed with a precision of 10%.

To conduct very high currents, the busbar must provide sufficient cooling to the terminals. Simulations were done for IHM A and IHM B with  $T_H=80^\circ\text{C}$  and an interface temperature  $T_B$  of  $60^\circ\text{C}$ . In this case, the maximum temperature  $T_{max}$  is no longer reached at the top of the terminals but at their center region.  $T_{max}$  as a function of current  $I$  per IHM system was extracted from ANSYS modelling and is plotted in Figure 13.

With any given maximum temperature for module reliability, it can be clearly seen that the reduction of lead resistance  $R_{lead}$  and the improved thermal coupling to the heatsink  $R_{thSC}$  have led to a significant increase in current carrying capability in the IHM B module.

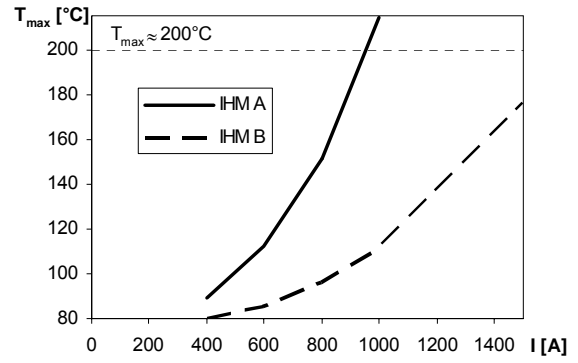


**Figure 13: Modelling of  $T_{max}(I)$  for IHM A and IHM B,  $T_H=80^\circ\text{C}$ ,  $T_B=60^\circ\text{C}$**

### Static self heating for a busbar

To determine the power dissipation from the busbar to the ambient, a model busbar with 3mm thick copper sheets and Rogers R 8124.2 insulation was prepared. The busbar has the same width as one system of an IHM-module, so the results can be applied to an entire module by paralleling. The busbar is shown in Figure 14.

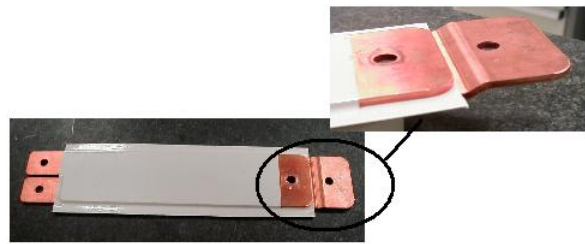


**Figure 14: Model busbar for measurements**

Taking into account that a busbar will find its equilibrium between the resistive dissipation of the  $I^2R$  heat generation and the heat transfer caused by both convection and conduction, we can calculate the temperature rise of the busbar used within this study. The maximum temperature rise  $\Delta T$  is calculated by: [1, 2]

$$\Delta T_{max} = \frac{I^2 \cdot R \cdot B}{K_{eav} \cdot A_s} = 18.7^\circ\text{C} \quad (2)$$

where  $I$  = current [A]  
 $R$  = resistance [ $\Omega$ ]  
 $B$  = boundary layer thickness [cm]  
 $K_{eav}$  = thermal conductivity of air [W/cmK]  
 $A_s$  = surface area of busbar

The temperature rise for a laminated busbar is mainly driven by cross section and current. Practical measurement results are shown in Figure 15. The equilibrium value as given by (2) is reached after one hour.

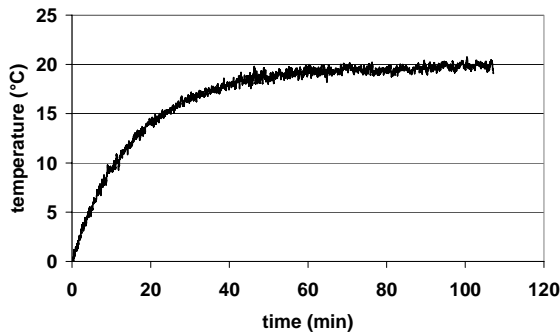


Figure 15: Static self heating for the busbar used in this study,  $I=440A$

For the design, inhomogeneity of  $T$  across the busbar must also be considered. Measurements have shown that hot spots occur at the terminal connections. Information can be gathered from infrared images as shown in Figure 16.

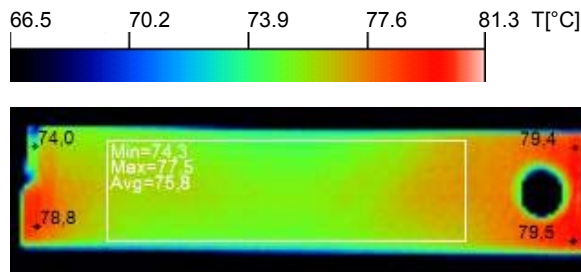


Figure 16: Temperature distribution across the busbar, infrared image

### Transient behaviour of IHM module and busbar assembly

For the inverter design, the transient thermal behavior of the assembly may be considered to avoid oversizing the busbar. In traction applications for example, peak currents may occur for a limited time only, and if the thermal capacity of the busbar is large enough, it can be designed for lower static currents. The behavior of the entire system is measured with the model busbar fitted to the experimental modules as described above. We carry out transient measurements with a representative current cycle of 500A for 30s, 200A for 30s, 600A for 20s and no current for 20s. This corresponds to an rms current of  $I=400A$  when resistances are assumed to be temperature independent. The cycle is run twice to see the long-term development. Before and after the cycle a constant current is applied, resulting in stationary conditions. Temperature data is acquired every 2s. The result is shown in Figure 17. The overall decrease in temperature is due to the initial

current of 470A, which was higher than the rms current of the cycle. While the terminal screw shows a ripple of  $2^{\circ}C$ , the busbar capacity buffers the ripple completely. Designing for the static load would be permissible in this case.

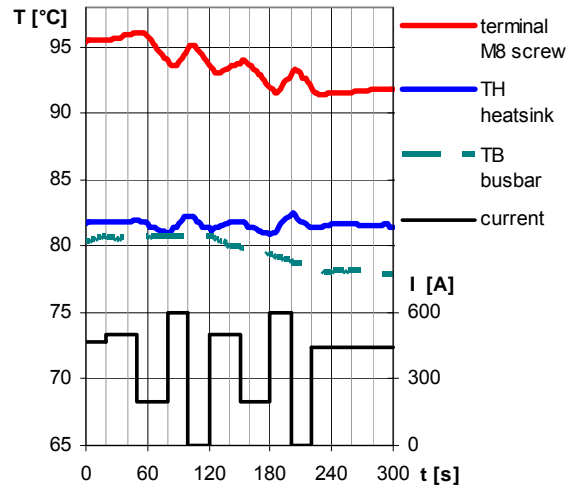


Figure 17: Transient behaviour of one IHM B system with busbar, ambient temperature  $22^{\circ}C$

### Summary

In this work we have discussed different internal structures of power terminals and the thermal behaviour of the module and busbar assembly. We have shown that bond wire connections of power terminals is adequate for medium power modules if the wires are kept short and if they are placed directly on the substrate to enhance cooling. For high power modules, solder technology is preferred. Current carrying capability is increased sharply from the IHM A module to the IHM B module by changing the internal layout of the power terminals. We have given static design criteria for the busbar and have shown that they are sufficient for typical transient states in traction applications.

### References

- [1] S. J. Raffles et al, **Calculating Temperature Rise in Bus Bars**, Rogers Corporation Power Distribution Division, 1989.
- [2] S. Van Acker, **Predictability of the Behavior of Power Distribution Components in Power Conversion Applications**, PCIM Shanghai 2004.
- [3] A. Cosaert, **Static self heating on Busbars, 1832/006/00: Busbar and IGBT related Parameters**, October 2003.

**Busbar Division**

Afrikalaan 188

B-9000, Gent, Belgium

Phone: +32-9-235-36-11

Fax: +32-9-235-36-58

[www.rogerscorporation.com](http://www.rogerscorporation.com)